

## Imperfection Effects for Multiple Applications of the Quantum Wavelet Transform

M. Terraneo and D. L. Shepelyansky

*Laboratoire de Physique Quantique, UMR 5626 du CNRS, Université Paul Sabatier, 31062 Toulouse Cedex 4, France\**  
(Received 10 March 2003; published 26 June 2003)

We study analytically and numerically the effects of various imperfections in a quantum computation of a simple dynamical model based on the quantum wavelet transform. The results for fidelity time scales, obtained for a large range of error amplitudes and number of qubits, imply that for static imperfections the threshold for fault-tolerant quantum computation is decreased by a few orders of magnitude compared to the case of random errors.

DOI: 10.1103/PhysRevLett.90.257902

PACS numbers: 03.67.Pp, 03.65.Yz, 03.67.Lx, 05.45.Mt

The mathematical theory of wavelet transforms (WT) is currently finding an enormous success in various fields of science and technology, including treatment of large databases, data and image compression, signal processing, telecommunications, and many other applications [1,2]. Wavelets are obtained by translations and dilations of an original function and they allow one to obtain high resolutions of microscopic details, both in frequency and space. The discrete WT can be implemented with high computational efficiency and provide a powerful tool for treatment of digital data. It is well accepted that the Fourier transform and WT are the main instruments for data treatment, and it has been shown that in many applications the performance of WT is much higher compared to the Fourier analysis. The permanent growth of computer capacity has significantly increased the importance of the above transformations in numerical applications.

The recent development of quantum information processing has shown that computers based on laws of quantum mechanics can perform certain tasks exponentially faster than any known classical computational algorithms (see, e.g., [3]). The most known example is the integer factorization algorithm proposed by Shor [4]. An essential element of this algorithm is the quantum Fourier transform (QFT) which can be performed for a vector of size  $N = 2^{n_q}$  in  $O(n_q^2)$  quantum gates, in contrast to  $O(2^{n_q} n_q)$  classical operations [3,4]. Here  $n_q$  can be viewed as the number of qubits (two-level quantum systems) of which a quantum computer is built. Apart from Shor's algorithm, the QFT finds a number of various applications in quantum computation, including the simulation of quantum chaos models showing rich and complex dynamics [5–7]. The sensitivity of the QFT to imperfections was tested in numerical simulations and the time scales for reliable computation of the algorithm were established [6–9].

A few years after the discovery of the QFT algorithm, it has been shown that certain WT can also be implemented on a quantum computer in a polynomial number of quantum gates [10–12]. In fact, explicit quantum circuits were developed for the most popular discrete WT,

namely, the 4-coefficient Daubechies WT [ $D^{(4)}$ ] and the Haar WT, both for pyramidal and packet algorithms [10–12]. As it happens in classical signal analysis, it is natural to expect that QWT will find important future applications for the treatment of quantum databases and quantum data compression. Therefore, it is important to investigate the stability and the accuracy of QWT in respect to imperfections. This is especially important since the functions of the wavelet basis have singularities in the derivatives (in contrast to analyticity of Fourier waves) that may enhance the effects of perturbations.

To this aim we introduce a simple model with rich nontrivial dynamics which is essentially based on multiple applications of the WT. Its quantum evolution can be efficiently simulated on a quantum computer, and it is described by the unitary map for the wave function  $\psi$ :

$$\bar{\psi} = \hat{U}\psi = \hat{W}^\dagger e^{-ik(x-\pi)^2/2} \hat{W} e^{-iTn^2/2} \psi. \quad (1)$$

Here the bar marks the value of the wave function after one map iteration,  $\hat{W}$  is the  $D^{(4)}$  WT operator, and the unitary diagonal operators  $U_T = e^{-iTn^2/2}$  and  $U_k = e^{-ik(x-\pi)^2/2}$  represent quantum phase rotation in computational and wavelet basis, respectively. The evolution takes place in the Hilbert space of  $N = 2^{n_q}$  states, with  $-N/2 \leq n < N/2$  and  $x = 2\pi j/N$  where  $j = 0, \dots, N-1$  is the index in the wavelet basis and  $T, k$  are dimensionless parameters. In the case when  $\hat{W}$  is replaced by the Fourier transform, one obtains the quantum sawtooth map previously analyzed in Ref. [7]. Thus the model (1) can be considered as a “kicked wavelet rotor,” where  $k$  is the kick strength in the wavelet basis.

The global properties of the evolution operator (1) are shown in Figs. 1 and 2 for different values of  $k$ . The density plot of transition matrix elements  $U_{n,n'}$  in the computational basis is represented in Fig. 1. By increasing  $k$  a larger and larger number of states is coupled by the dynamics, and the complex self-similar structure of the transitions generated by the WT becomes evident. On the average, the off-diagonal matrix elements decay with the power law  $|U_{n,n'}|^2 \sim 1/|n-n'|^\alpha$ . Asymptotically for  $|n-n'| \gg 5k$  we obtain the exponent

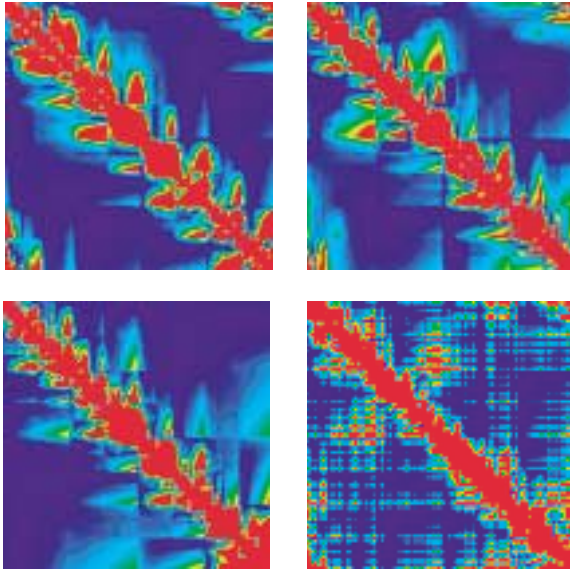


FIG. 1 (color online). Density plot of matrix elements  $|U_{n,n'}|^2$  for the model (1) in the computational basis, for  $N = 2^{12}$ . Top:  $k = 100$  (left),  $k = 1000$  (right); bottom is for  $k = 1000$ : a doubled resolution of left upper quarter (left), perturbed operator with static errors  $\epsilon = 5 \times 10^{-4}$ ,  $\mu = 0$ . Color marks the density from blue (zero) to red (maximal value).

$\alpha = 4$  (Fig. 2). For large values of  $k$  the intermediate scaling law is described by the exponent  $\alpha = 2$ , in the range  $1 \leq |n - n'| \ll 5k$ . This decay law for the matrix elements can be considered as a long range coupling between states. We note that similar power law regimes have been analyzed in random matrix models [13,14]. Our numerical analysis shows that there are two regimes for the level spacing statistics  $P(s)$  [15] in the limit of

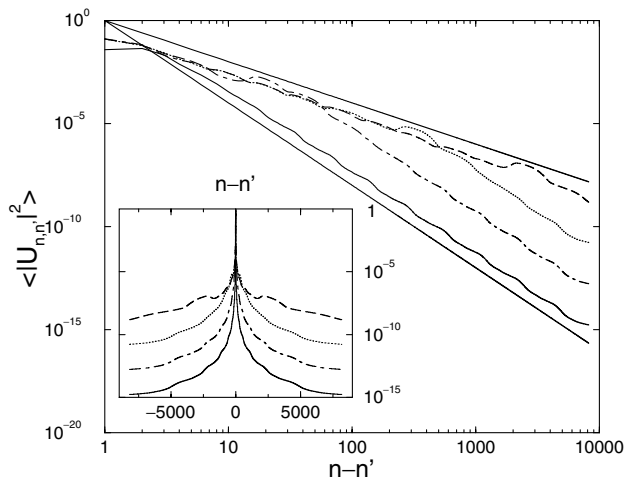


FIG. 2. Dependence of averaged matrix elements  $\langle |U_{n,n'}|^2 \rangle$  on  $|n - n'|$  (the average is taken along the diagonal). Data are shown for  $N = 2^{15}$  and  $k = 1$  (full black curve),  $k = 10$  (dash-dotted curve),  $k = 100$  (dotted curve), and  $k = 1000$  (dashed curve). The two straight lines are  $1/|n - n'|^2$  and  $1/|n - n'|^4$ . The inset shows the data in semilog scale.

large  $N$ . E.g., for  $N = 2^{12}$  the distribution  $P(s)$  is given by the Poisson law for  $k < 5$ , while for  $5 < k \leq 10000$  it shows level repulsion and a Poissonian decay for large  $s$  (data not shown). We attribute the rapid appearance of level repulsion to the slow power law decay of matrix elements [14].

To implement the evolution (1) on a quantum computer, we developed an algorithm based on the QWT for the Daubechies  $D^{(4)}$  wavelets. The algorithm consists of four steps: (i) the multiplication by  $\hat{U}_T$ , performed in  $O(n_q^2)$  controlled-phase shift gates as described in [7]; (ii) the application of  $\hat{W}$  operator, realized by the QWT following the circuit described in Fig. 10 of [11](see details in [16]); (iii) the operator  $\hat{U}_k$ , implemented in a similar way as for the step (i); (iv) the inverse WT  $\hat{W}^\dagger$ , obtained by reversing the gates of the step (ii). The heaviest parts of the algorithm are the steps (ii), (iv), since the QWT algorithm requires multicontrolled operations. To implement them we used the recipe given in [17] which allows one to realize a  $n$ -controlled gate by  $O(n)$  elementary gates (Toffoli and 1- and 2-qubit gates). To this end an ancilla qubit is needed, so that we used  $n_q + 1$  qubits to simulate numerically the dynamics of model (1) with  $N = 2^{n_q}$  states. The implementation of the wavelet kernel  $D_{2^n}^{(4)}$  requires  $O(n)$  multicontrolled gates ( $n = 2, \dots, n_q$ ), and since the QWT is composed of  $O(n_q)$  kernel applications this leads the total number of elementary gates to scale as  $O(n_q^3)$  [10–12]. To study the algorithm accuracy we consider two models of imperfections. In the model of random noisy gates we replace all ideal gates by imperfect ones, which are obtained by random unitary rotations by a small angle  $\eta$ ,  $-\epsilon/2 \leq \eta \leq \epsilon/2$ , around the ideal rotation angle (as in [18]). In the model of static imperfections (see [7,19]) all gates are perfect but between gates  $\psi$  accumulates a phase factor  $e^{i\phi}$  with  $\phi = \sum_l (\eta_l \sigma_l^z + \mu_l \sigma_l^x \sigma_{l+1}^x)$ . Here  $\eta_l, \mu_l$  vary randomly with  $l = 0, \dots, n_q$ ,  $\eta_l$  represents static one-qubit energy shifts,  $-\epsilon/2 \leq \eta_l \leq \epsilon/2$ , and  $\mu_l$  represents static interqubit couplings on a circular chain,  $-\mu/2 \leq \mu_l \leq \mu/2$ .

The numerical simulations of the ideal quantum algorithm for the map (1) show that the wave function is essentially localized on a few states of the computational basis. This localization is clearly seen from the inverse participation ratio (IPR)  $\xi = 1/\sum_n |\psi_n|^4$  which is a standard quantity to characterize localization in mesoscopic systems [15]. It directly provides the number of sites on which the probability is concentrated. Surprisingly the localization is present not only for moderate  $k \sim 1$ , but also when the kick strength is very large  $k \sim 1000$  (see Fig. 3). Indeed in both cases  $\xi$  fluctuates near a constant value  $\xi_0 \ll N$ , even for a very large number of iterations. We attribute this localization to the structure of the operator (1): it is banded for moderate  $k$  and sparse for large  $k$  (see Fig. 1). For  $k \sim 1$  the probability shows an algebraic localization  $|\psi_n|^2 \propto 1/n^4$  (Fig. 4). Such an exponent fully agrees with the scaling law of Fig. 2. For  $k > 100$ , the probability is spread over the whole basis (data

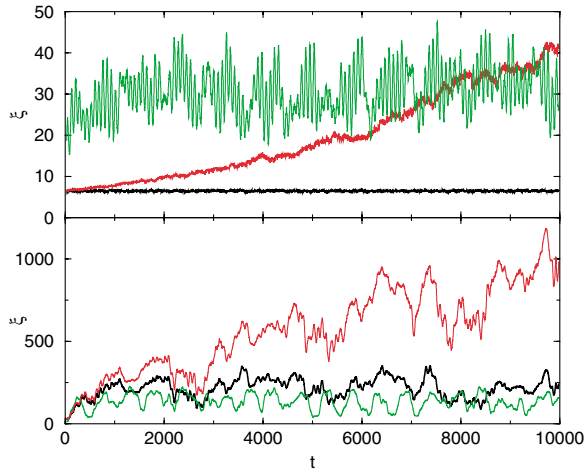


FIG. 3 (color online). Dependence of IPR  $\xi$  on the number of iterations  $t$ , for  $n_q = 12$ ,  $T = 1.4$ ,  $k = 1$  (top), and  $k = 1000$  (bottom). Initially the probability is concentrated at  $n = 0$ . The black curves show the quantum computation with ideal gates; the green (light gray) curves show the case with static errors at  $\epsilon = 10^{-4}$ ,  $\mu = 0$  and red (gray) curves correspond to the case with noisy gates at  $\epsilon = 5 \times 10^{-4}$ . The data are averaged over time interval  $\Delta t = 50$ .

not shown), but only a moderate number of narrow peaks contributes to the IPR value (see Fig. 3). This behavior is consistent with the fact that the  $P(s)$  never reaches a Wigner-Dyson regime (see discussion above). On the contrary, the spectral properties of the sawtooth map [7,20] are described by the random matrix theory for  $k \sim 1000$ ,  $T \sim 1$ , and  $N = 2^{12}$ .

The effect of imperfections in the quantum gates is shown in Figs. 3 and 4. The results clearly show that the localization is destroyed by noisy gates imperfections

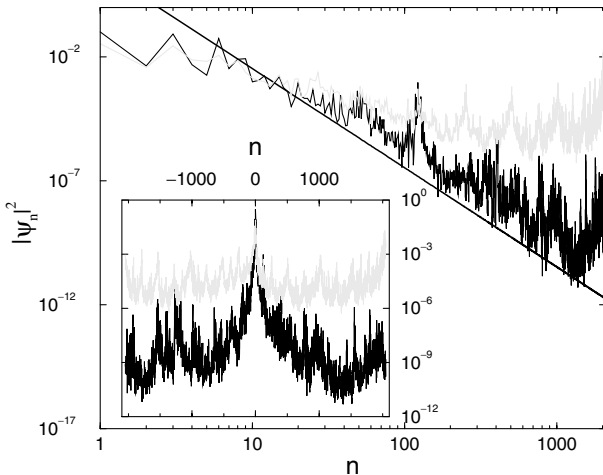


FIG. 4. Probability distribution  $|\psi_n|^2$  in the computational basis for the parameters of Fig. 3 (top) at  $k = 1$ ,  $t = 10^4$ : full curve is the quantum computation with ideal gates, gray curve shows data for noisy gates with  $\epsilon = 5 \times 10^{-4}$ . The straight line displays the scaling law  $1/n^4$ . The inset shows the same data in semilogarithmic scale.

which lead to an approximately linear growth of  $\xi$  with  $t$ . For static imperfections  $\xi$  shows modified bounded oscillations. The probability distribution in Fig. 4 shows the appearance of a plateau with pronounced peaks located approximately at  $n = N/2^m$ ,  $m = 1, 2, 3 \dots$ . We attribute the appearance of these peaks to the pyramidal structure of the algorithm, which in the presence of imperfections produces stronger errors at the above values of  $n$ . For static imperfections the plateau level remains bounded in time  $t$  while for noisy gates it increases with  $t$  and for very large  $t$  the probability becomes homogeneously distributed over the computational basis.

The qualitative difference between two types of imperfections becomes clear from the analysis of the behavior of the fidelity, defined as  $f(t) = |\langle \psi_\epsilon(t) | \psi(t) \rangle|^2$ . Here  $\psi(t)$  is the wave function obtained with ideal gates, while  $\psi_\epsilon(t)$  is the result of the quantum computation with imperfections of amplitude  $\epsilon$ . We determine the time scale  $t_f$  for accurate computation by fixing a threshold for the fidelity as  $f(t_f) = 0.9$ . In this way it is possible to find the dependence of  $t_f$  on the system parameters. Our numerical data are presented in Fig. 5. They show that for noisy gates  $t_f$  is described by the relation

$$t_f = C/(\epsilon^2 n_g), \quad N_g = C/\epsilon^2, \quad (2)$$

where  $n_g$  is the number of gates per map iteration,  $N_g = n_g t_f$  is the total number of gates, and  $C \approx 5$  is a numerical

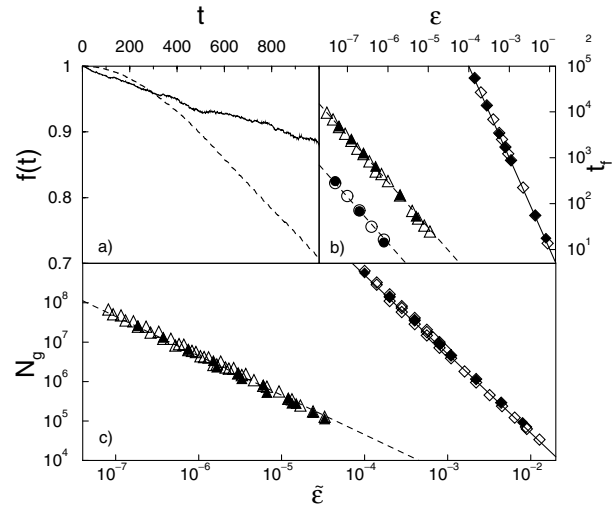


FIG. 5. Panel (a) shows the fidelity decay in time at  $k = 1$ ,  $n_q = 12$  for static imperfections ( $\epsilon = 10^{-4}$ ,  $\mu = 0$ , dashed curve) and noisy gates ( $\epsilon = 5 \times 10^{-4}$ , full curve). Panel (b) shows the dependence of time scale  $t_f$  on the imperfection strength  $\epsilon$  for  $n_q = 8$  ( $n_g = 5237$ ) for noisy gates (diamonds) and static imperfections (triangles at  $\mu = 0$ ; circles at  $\mu = \epsilon$ , for clarity data are shifted in  $\epsilon$  axis by a factor 10 to the left). Panel (c) gives the dependence of the total number of gates  $N_g$  on  $\tilde{\epsilon}$  for  $n_q = 6, 8, 10$ . For noisy gates (diamonds)  $\tilde{\epsilon} = \epsilon$  and for static imperfections (triangles)  $\tilde{\epsilon} = \epsilon \sqrt{n_q}$ . Open (full) symbols are data for  $k = 1$  ( $k = 1000$ ). The full and dashed lines in panels (b),(c) show the relations (2) and (3), respectively.

constant. The physical origin for this scaling is related to the fact that after each gate an amount of probability of the order of  $\epsilon^2$  is transferred from the ideal state to all other states. This leads to an exponential decay of the fidelity  $f(t) \approx \exp(-A\epsilon^2 n_g t)$ , where  $A$  is a constant [see Fig. 5(a)]. This gives the scaling (2), which was also found in other algorithms with noisy gates [7,9,18].

For the model with static imperfections the scaling is

$$t_f = D/(\epsilon n_g n_q^{1/2}), \quad N_g = D/(\epsilon n_q^{1/2}), \quad (3)$$

where  $D$  is a numerical constant ( $D \approx 4.5$ , at  $\mu = 0$  and  $D \approx 2.1$  at  $\mu = \epsilon$ ). This time scale is significantly smaller than the one for noisy gates. Physically, this happens due to the coherent action of static imperfections, which lead to effective Rabi oscillations proportional to  $\cos(\epsilon n_g t)$  for each qubit. For  $n_q$  qubits this gives  $f(t) \propto [\cos(\epsilon n_g t)]^{n_q}$  and for small  $\epsilon$  we obtain a Gaussian drop of the fidelity  $f(t) \sim \exp[-n_q(\epsilon n_g t)^2]$ , in agreement with our numerical results [see Fig. 5(a)]. This leads to the scaling (3), which is confirmed by the data in Fig. 5. The effects of static imperfections are dominant for all range of imperfection strengths studied. We note that similar scalings were discussed and numerically demonstrated in other quantum algorithms with noisy gates [9,18] and static imperfections [7](see also [21]). This shows that such scaling laws are generic and are not sensitive to the singularities in the derivatives of the wavelets. The universality of the above relations (2) and (3) is also confirmed by the fact that the structure of the QWT is rather different from the QFT algorithm, e.g., the number of elementary quantum gates scales as  $O(n_q^3)$  for the QWT, in contrast to  $O(n_q^2)$  for the QFT. These relations determine the total number of gates  $N_g = t_f n_g$  during which the quantum computation is reliable. Similar scalings for  $N_g$  should also be valid for other quantum algorithms, e.g., Grover's and Shor's algorithms.

The above relations (2) and (3) are important for the quantum error correction codes and the fault-tolerant quantum computation threshold (see [3,22], and references therein). Indeed the accuracy border for large scale quantum computation is obtained in the assumptions of random noisy errors and gives a threshold  $\epsilon < \epsilon_r \sim 10^{-2}$ . This approach intrinsically uses the fact that for noisy gates the fidelity remains close to 1 for a number of gates  $N_g = C/\epsilon_r^2$  [see (2)]. In the case of static imperfections it is natural to assume that this number of gates should remain approximately the same to allow large scale computation on a quantum computer with  $n_q$  qubits. Therefore, for static imperfections Eqs. (2) and (3) give the accuracy border  $\epsilon_s$ :

$$\epsilon_s \approx D\epsilon_r^2/(Cn_q^{1/2}). \quad (4)$$

This important relation gives a significant decrease of the threshold for the case of static imperfections [23]. For the parameters of our model at  $n_q = 10$  we obtain that for the noisy error rate  $p_r = \epsilon_r^2 \approx 10^{-4}$  the rate induced by

static imperfections should be less than  $p_s = \epsilon_s^2 \approx 10^{-9}$ . This result shows that new strategies of quantum error correction codes should be developed to significantly suppress phase shifts induced by static imperfections. The spin echo techniques used in NMR [3] may play here an important role.

This work was supported in part by the EC Contracts No. RTN QTRANS and No. IST-FET EDIQIP and the NSA and ARDA under ARO Contract No. DAAD19-01-1-0553. We thank CalMiP in Toulouse and IDRIS at Orsay for access to their supercomputers. We thank D. Gottesman for discussions.

\*Electronic address: <http://www.quantware.ups-tlse.fr>

- [1] I. Daubechies, *Ten Lectures on Wavelets*, CBMS-NSF Series in Applied Mathematics (SIAM, Philadelphia, 1992).
- [2] Y. Meyer, *Wavelets: Algorithms and Applications* (SIAM, Philadelphia, 1993).
- [3] M. A. Nielsen and I. L. Chuang, *Quantum Computation and Quantum Information* (Cambridge University Press, Cambridge, 2000).
- [4] P. W. Shor, in *Proceedings of the 35th Annual Symposium on Foundation of Computer Science*, edited by S. Goldwasser (IEEE Computer Society, Los Alamitos, California, 1994), p. 124.
- [5] R. Schack, *Phys. Rev. A* **57**, 1634 (1998).
- [6] P. H. Song and D. L. Shepelyansky, *Phys. Rev. Lett.* **86**, 2162 (2001).
- [7] G. Benenti *et al.*, *Phys. Rev. Lett.* **87**, 227901 (2001).
- [8] J. I. Cirac and P. Zoller, *Phys. Rev. Lett.* **74**, 4091 (1995).
- [9] C. Miquel, J. P. Paz, and W. H. Zurek, *Phys. Rev. Lett.* **78**, 3971 (1997).
- [10] P. Hoyer, quant-ph/9702028.
- [11] A. Fijaney and C. Williams, *Lecture Notes in Computer Science* (Springer, Berlin, 1998), No. 1509, p. 10; quant-ph/9809004.
- [12] A. Klappenecker, in *Wavelet Applications in Signal and Image Processing VII*, edited by M. A. Unser, A. Aldroubi, and A. F. Laine, SPIE Proceedings (SPIE—International Society for Optical Engineering, Bellingham, WA, 1999), p. 703.
- [13] J. P. Bouchaud and A. Georges, *Phys. Rep.* **195**, 127 (1990).
- [14] A. D. Mirlin *et al.*, *Phys. Rev. E* **54**, 3221 (1996); M. L. Ndawana and V. E. Kravtsov, cond-mat/0302569.
- [15] A. Mirlin, *Phys. Rep.* **326**, 259 (2000).
- [16] M. Terraneo and D. L. Shepelyansky, quant-ph/0303043.
- [17] A. Barenco *et al.*, *Phys. Rev. A* **52**, 3457 (1995).
- [18] B. Georgeot and D. L. Shepelyansky, *Phys. Rev. Lett.* **86**, 5393 (2001).
- [19] B. Georgeot and D. L. Shepelyansky, *Phys. Rev. E* **62**, 3504 (2000); **62**, 6366 (2000).
- [20] G. Benenti *et al.*, *Eur. Phys. J. D* **20**, 293 (2002); **22**, 285 (2003).
- [21] W. H. Zurek, *Phys. Rev. Lett.* **53**, 391 (1984); V. V. Flambaum, *Aust. J. Phys.* **53**, 489 (2000).
- [22] A. Steane, quant-ph/0207119.
- [23] D. Gottesman (personal communication).